Enhanced proportional integral controller for DSTATCOM with particle swarm optimization algorithm in power system

Parag Vijay Datar, Deepak Balkrishna Kulkarni
Department of Electrical and Electronics Engineering, KLS Gogte Institute of Technology,
Under Visvesvaraya Technological University, Belagavi, India

Article Info

ABSTRACT

Power system expansion planning is supported by using distributed generation (DG) instead of installing new main power system generators. The portability and autonomous operation of the DG make it capable of integrating into the distribution system. Power electronics devices for home loads, mainly electric vehicles, mobile phones, and laptops, introduce harmonics and related power quality issues to the distribution system. This load creates power quality issues like an increase in total harmonic distortion (THD) and a reduction in power factor. This paper uses the DG to supply important power electronics devices for the mitigation of power quality problems in distributed systems with non-linear loads, such as electric vehicles, called the "distributed static compensator (DSTATCOM)". Wind and photovoltaic (PV) generators supply power to a common DC source. To improve power quality D-STATCOM powered by PV and wind energy systems at the DC link is incorporated. The direct axis/quadrature axis method (DQ method) controls the real and reactive components of the power. Proportional integral (PI) and particle swarm optimization (PSO) based PI controller parameter estimation are developed, and results are compared for power quality performance. In terms of improving power quality, the PSO-based parameter estimate of the PI controller performs better than the traditional PI controller.

Corresponding Author:

Parag Vijay Datar
Department of Electrical and Electronics Engineering, KLS Gogte Institute of Technology
Under Visvesvaraya Technological University,
Udyambag, Belagavi, Karnataka, India
Email: pvdatar@git.edu

1. INTRODUCTION

The distribution system's distributed static compensator (DSTATCOM), which has been positioned strategically, efficiently controls reactive power by making use of the inverter's stochastic behavior. It functions as a shunt compensator and is smoothly connected across the distribution system's load, allowing it to switch between acting as a source and a sink of reactive power as necessary. In order to offset reactive power disturbances brought on by load-side disruptions in distribution networks, DSTATCOM is effectively used. Power electronic components used to power diverse DC loads cause non-linearities to be introduced into the distribution system. As a result, a variable AC power source is required to reduce the distribution system's reactive power non-linearity. The transmission of reactive disturbances to the distribution source is effectively prevented by the use of DSTATCOM. The load-induced non-linearities (reactive power) are compensated for by the shunt compensation current, which ensures that they are reduced before reaching the distribution source.

The proportional integral (PI) controller has two independent parameters (proportional and integral gain), Kp and Ki. These gains are adjusted to obtain the dynamic control of the DSTATCOMS. Parameter estimation using different meta-heuristic methods like particle swarm optimization (PSO) is needed to obtain these gains to be having a better dynamic response to disturbance in the distribution system [1], [2]. DSTATCOM uses a synchronous reference frame (SRF)-based controller to inject current that can compensate for the non-linear current from the load. The distribution system source has to be maintained without disturbance since it is connected to other loads as well so that other loads are not affected [3]. The total harmonic distortion (THD) of the source current is found to be improved by introducing the DSTATCOM at the point of common coupling (PCC). Since DSTATCOM acts as the variable AC source, it is an application of highly stochastic power electronic devices like matrix converters. A model predictive controller (MPC) is used to develop the DSTATCOM using the matrix converter with an inductive storage element [4]. Photovoltaic (PV) generator is integrated into the power system using the two-level inverter acting as the DSTATCOM using the modified SRF controller [5]. A microgrid with PV and wind generators is controlled for improved voltage stability. This autonomous microgrid system uses voltage stability as the objective and tunes the PI controller using genetic algorithms (GA) and bacterial foraging algorithms (BFA) [6]. The best locations for the PV array and DSTATCOM within a distribution system are chosen using the fuzzy lightning search algorithm.

The distribution system's buses with the best locations for PV and DSTATCOM are identified using this approach [7]. Artificial intelligence approaches are used in power system-connected systems to regulate real and reactive power. The real and reactive power are specifically controlled by a PV-integrated system [8]. Both static VAR compensator (SVC) and DSTATCOM are used for voltage sag enhancement in hybrid PV-wind power system-connected systems [9]. Since the primary power system does not support the microgrid, the voltage stability in the microgrid environment must be supported by external devices like DSTATCOM. The voltage regulation using the DSTATCOM on the microgrid is satisfactory [10]. Recently in power systems, multilevel inverters are utilized to mitigate harmonic distortions caused by load disturbances at the source. Instead of two-level inverters, multilevel inverters are used in the DSTATCOM voltage source inverter (VSI), which comprises the topology with a reduced number of switches [11], [12]. Although advanced maximum power point tracking (MPPT) algorithms are introduced in the PV generators [13] with reinforced learning and sliding mode control, the DSTATCOM controls the power using the PWM control in the VSI. Different topologies of DSTATCOM, like the three-phase, four-switch converter concept implemented in [14], self-supported transformer-less DSTATCOM [15], and intelligent battery control [16], are available. Literature has reviewed different PV-integrated [17] DSTATCOM implementations [18], sliding mode control of PV system [19] DSTATCOM with active power filter and dual active technology [20], solar modeling techniques [21], power system integration of PV [22], and muti-objective-based power system integration systems [23], [24] and MPPT algorithms [25].

Although previous literature [1], [2], [6] has used PSO-PI to control DSTACOM dynamically, the objectives are real and reactive power improvement and transient voltage improvement; in this paper, a PV-powered DSTATCOM is controlled dynamically using PSO-PI controller to improve power quality in the power system with different non-linear loads. A comparison between the PI controller and the PSO-tuned PI controller is done to determine the viability. Based on power quality and stability, the evaluation takes into account power curves under fault-and unbalanced-loading-related scenarios.

2. METHOD
2.1. Dynamic control of harmonics using PSO-PI controller

A two-bus topology is considered for the implementation with the rating of the Indian power distribution system of 440 V, and 50 HZ. PV and wind power generation are implemented at the DC link for real power support for DSTATCOM. Figure 1 illustrates the control scheme for the DSTATCOM, where the PV power generation is linked to a boost converter, and a perturb and observe (P&O) MPPT technique is utilized to supply DC power to the DC link of the VSI. Additionally, the wind generator, equipped with a permanent magnet synchronous motor (PMSM) drive, is connected to the rectifier. The MPPT controller regulates the boost converter to provide the DC link voltage to the VSI. Figure 2 illustrates the entire setup for power quality disturbance reduction using the MPPT perturb and observe algorithm. The proposed implementation develops the mitigation in power system-connected PV distributed using two loops: the power system synchronization loop and a power quality disturbance mitigation loop, as shown in Figure 2. The P&O method is used to generate pulses in the MPPT control feed-forward loop, which regulates the boost converter. The DC link, which is powered by a power system-integrated three-level inverter run on multicarrier space vector pulse width modulation (SVPWM), receives power from the boost converter's

output. The inverter has to handle the power quality problems created by these loads. Voltage and current from the inverter output are decoupled to obtain the SRF components.

A VSI is used to convert the DC power to AC electricity. The distribution system can be linked to the VSI's output via an LC filter and PCC. When distribution system synchronization is performed, keeping track of distribution system code parameters is crucial. Phase-locked loop (PLL)-based DSTATCOM is effective for delivering power with good power quality. SRF-PLL is the name given to the phase locking since it takes place in the orthogonal domain SRF-PLL. The complexity of phase locking is raised by noise, distortions, and frequency variations. SRF-PLL is the most advanced method utilized in three-phase systems SRF-PLL. Three-phase inverter analysis and control design heavily rely on the direct axis/quadrature axis (DQ) rotating frame transformation, which entails switching between stationary and rotating frames. The integrator and proportional component coupled in parallel together make up the PI controller. The distribution system side active and reactive power regulation is managed by the control approach, maintaining a consistent DC link voltage and distribution system code compliance at the distribution system side converter's output. The flow schematic for the distribution system-side converter controller is shown in Figure 3.
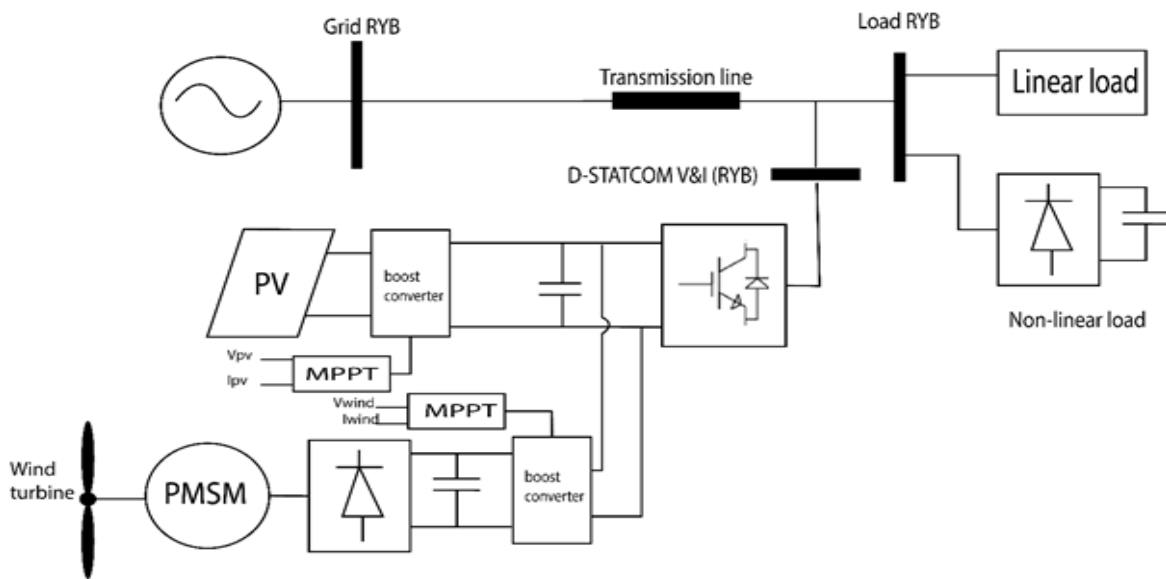

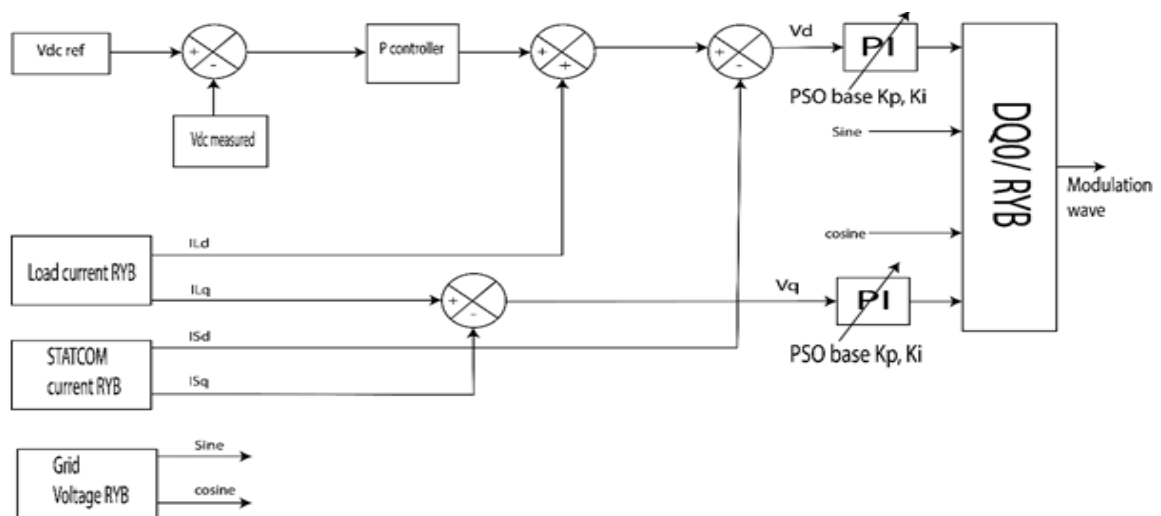Figure 1. Proposed block diagram of DSTATCOM with PV and wind sources

Figure 2. Proposed PSO-PI controller for distribution system integrsted STATCOM
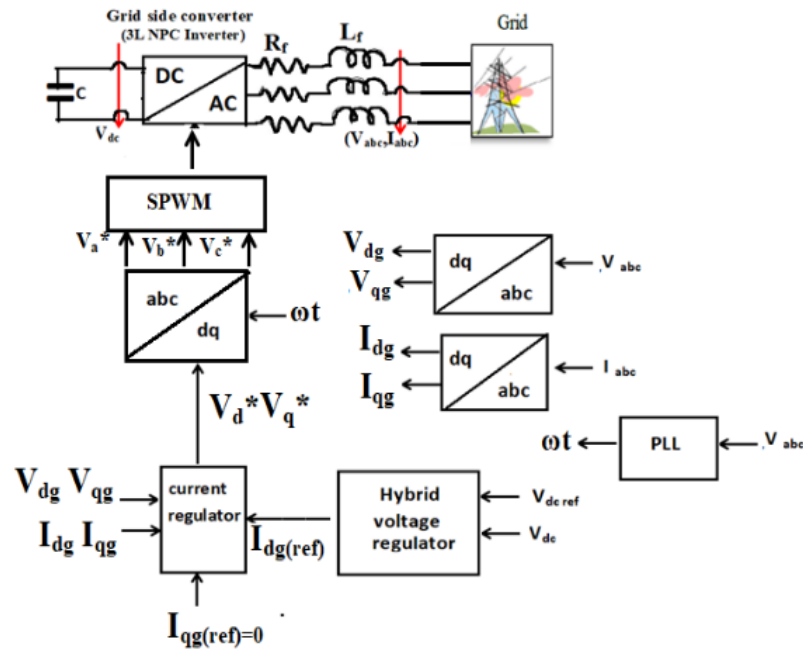
Figure 3. PLL based controller-distribution system side converter

The terminal voltage of the distribution system, respectively, Vabc and distribution system terminal current Iabc are determined using current and voltage sensors. A PLL, which is determined by (1), is used to detect the angle of the distribution system voltage. The transformation from abc to DQ or dq to abc uses this angle.

$$\omega = tan(\frac{V\beta}{V\alpha}) \tag{1}$$

$$V_\alpha = \frac{2}{3}\left(V_{ag} - 0.5V_{bg} - 0.5V_{cg}\right) \tag{2}$$

$$V_\beta = \frac{2}{3}(0.866V_{bg} - 0.866V_{cg}) \tag{3}$$

Where Vα and Vβ are the two-phase αβ components of distribution system voltage given by (2) and (3), Vag, Vbg, Vcg, and Vcg are the distribution system voltage components. The instantaneous three-phase AC voltages are represented by (4) to (6), using abc to dq conversion, these three-phase rotating voltage components V_{ag}, V_{bg}, and V_{cg} are converted into stationary components Vdg, Vqg, Vo as given by (7).

$$V_{ag} = V_p sin(\omega_t) \tag{4}$$

$$V_{bg} = V_p sin(\omega_t - 120^o) \tag{5}$$

$$V_{cg} = V_p sin(\omega_t + 120^o) \tag{6}$$

$$\begin{bmatrix} V_{dg} \\ V_{qg} \\ V_o \end{bmatrix} = \frac{3}{2}\begin{bmatrix} sin\omega t & sin(\omega t - 120^o) & sin(\omega t + 120^o) \\ cos\omega t & cos(\omega t - 120^o) & cos(\omega t + 120^o) \\ 0.5 & 0.5 & 0.5 \end{bmatrix}\begin{bmatrix} V_{ag} \\ V_{bg} \\ V_{cg} \end{bmatrix} \tag{7}$$

Similarly using abc to dq transformation, three-phase current components I_{ag}, I_{bg}, Icg are converted into stationary components I_{dg}, I_{qg}, I_0, as given by (8). Figure 4, shows the abc coordinate and dq coordinate frames using which the coordinate transform formulas are derived. Real and reactive power are calculated using the direct and quadrature axis components in (9) and (10).

$$\begin{bmatrix} I_{dg} \\ I_{qg} \\ I_o \end{bmatrix} = \frac{3}{2} \begin{bmatrix} sin\omega t & sin(\omega t - 120^o) & sin(\omega t + 120^o) \\ cos\omega t & cos(\omega t - 120^o) & cos(\omega t + 120^o) \\ 0.5 & 0.5 & 0.5 \end{bmatrix} \begin{bmatrix} I_{ag} \\ I_{bg} \\ I_{cg} \end{bmatrix} \qquad (8)$$
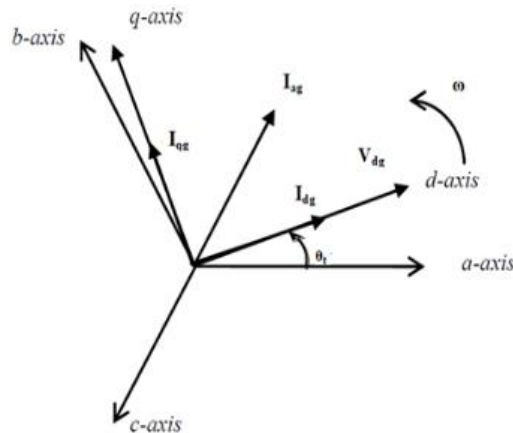

Figure 4. Three phase rotating frame from stationary frame transformation

$$P_{grid} = 1.5(V_{dg}I_{dg} + V_{qg}I_{qg}) \qquad (9)$$

$$Q_{grid} = 1.5(V_{qg}I_{dg} - V_{dg}I_{qg}) \qquad (10)$$

For the dynamic decoupling, the quadrature axis voltage Vqg is made to zero by aligning the direct axis component with the voltage space vector, which makes the quadrature axis component zero always. If the reference frame is Vqg=0, then the active and reactive power is given by (11) and (12), It is evident from (11), and (12), that the active and reactive powers are separately regulated by the d-axis current component Idg and the q-axis current component Iqg, respectively, for a given d-axis voltage. Figures 5 and 6 depict the d-axis and q-axis current regulators, respectively.

$$P_{grid} = 1.5V_{dg}I_{dg} \qquad (11)$$

$$Q_{grid} = -1.5V_{dg}I_{qg} \qquad (12)$$
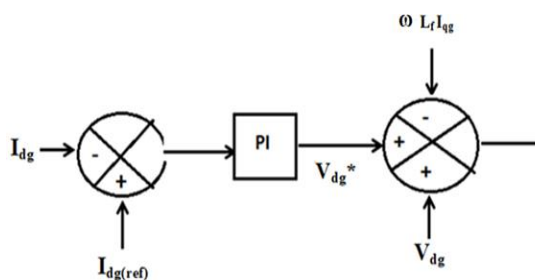

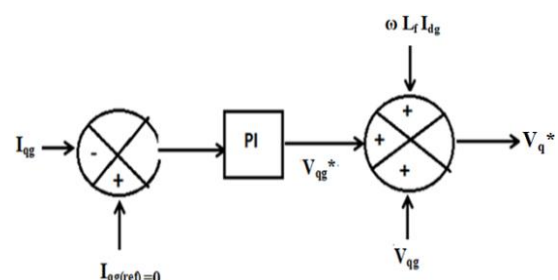Figure 5. D-axis current regulator   Figure 6. Q-axis current regulator

The d-axis reference current Idg (ref) has been generated by the PI regulator. The PI controller receives the discrepancy between the DC link voltage Vdc and the reference DC link voltage Vdc ref. The reactive power component is removed to reduce power system disruptions by setting the q-axis reference current Iqg (ref) to zero. In (13) and (14) describe the dq coordinate control equations that take the distribution system side line resistance Rf into consideration.

$$V_d *= V_{dg} * -\omega_t I_{qg} L_f + V_{dg} \tag{13}$$

$$V_q *= V_{qg} * +\omega_t I_{dg} L_f + V_{qg} \tag{14}$$

Vdg* and Vqg* are the reference voltage for the d-axis and q-axis voltages respectively given by (15) and (16), both direct axis and quadrature axis voltage are derived using the PI controller gain values. The aim of any controller is to tune the parameters of the controller such that any dynamics introduced in the can be handled by the controller.

$$V_{dg} *= (Kp + \frac{Ki}{s})(I_{dg(ref)} - I_{dg}) \tag{15}$$

$$V_{qg} *= (Kp + \frac{Ki}{s})(I_{qg(ref)} - I_{qg}) \tag{16}$$

The Vd* and Vq* components are then converted into three-phase time-varying AC components using dq to abc transformation as given in (17). This three-phase voltage comprises both the real and reactive power disturbances which needs to be nullified. Thus, this voltage is compared with the actual voltage and the difference voltage must be fed to the system.

$$\begin{bmatrix} V_a * \\ V_b * \\ V_c * \end{bmatrix} = \begin{bmatrix} sin(\omega t) & cos(\omega t) & 1 \\ sin(\omega t - 120^o) & cos(\omega t - 120^o) & 1 \\ sin(\omega t + 120^o) & cos(\omega t + 120^o) & 1 \end{bmatrix} \begin{bmatrix} V_d * \\ V_q * \\ 0 \end{bmatrix} \tag{17}$$

In the PWM controller, the signals Va*, Vb*, and Vc* are compared to triangular wave carrier signals to produce gate signals that activate the three-phase inverter switches. The DC link voltage and the Vdc ref error signal are inputs to the PI controller. Based on the values of Kp and Ki, the controller determines the Idg (ref) reference current. Refer to Figure 7 for a visual representation of this process.
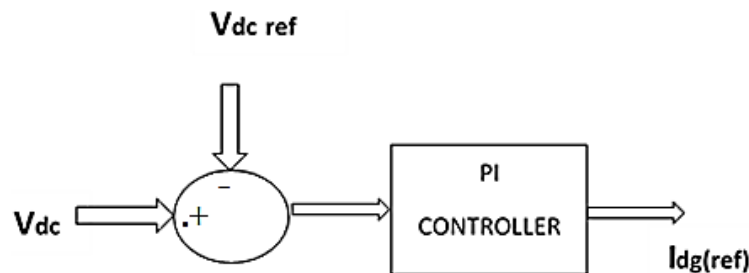

Figure 7. D-axis reference current generation using PI controller

Then the I_{Ld} error is given to the comparator with the DSTATCOM direct current (Isd) to derive direct voltage (Vd) using a PI controller. This PI controller is tuned by the PSO algorithm to optimize the controller gains Kp and Ki. On the other side, the load quadrature axis current (I_{Lq}) is compared with the DSTATCOM quadrature axis current (I_{Sq}). The compared quadrature current is converted to quadrature axis voltage using the PI controller. This PI controller is also tuned with the PSO algorithm. From the distribution system RYB measurement, the sine wave and cosine wave are generated using the PLL control. Using this V_d and V_q, the V_{RYB} is generated using DQO to RYB.

2.2. Conventional Ziegler-Nichol's method for PI controller

The Ziegler-Nichols method is a commonly employed technique for fine-tuning P, PI, and proportional–integral–derivative (PID) controllers. In this approach, the integral and differential gains are initially set to zero. Then, the proportional gain is incrementally increased until the system reaches instability. At the point where the system becomes unstable, the value of K_p is referred to as K_{max}, and the frequency of oscillation is denoted as f0. After that, the approach reduces the proportional gain by an amount that has been previously determined, and it configures the integral and differential gains so that they are functions of f0. The gains for P and D are adjusted (18) and (19).

$$K_p = 0.45\ K_{\{max\}} \tag{18}$$

$$K_I = 1.2\ f_0 \tag{19}$$

After getting the new value of K_p and K_I place the values in the controller then ach ve the new $K_{\{max\}}$ and f_0. Then repeat it again till the response is better. With the obtained gain values the system is made to work with the derived gain values. The derived gain values are capable of managing the dynamics introduced in the system and power quality limits are maintained.

2.3. PSO tuned PI controller

A well-known and simple technique called PSO uses the particle's velocity as the updating equation. With kp and ki values as the independent variable, the PSO generates the values of both these gains to iterate such that there is power disturbance mitigation in the power system. The populated gain values are updated in the succeeding iterations such that there is a convergence towards the minimal THD and power factor. The optimization procedure is given in the form of the flowchart in Figure 8.
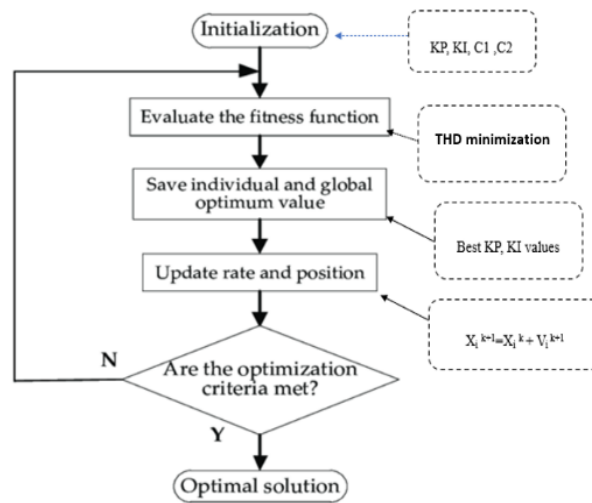

Figure 8. Flow chart particle swatrm optimization

The objective is to minimize the THD. The constraints are the inequality constraints of the kp and ki values. To get the objective, the simulation setup is run and then the THD value is obtained. The flow chart of the PSO algorithm, which is used for tuning the PI controller, is present as a flow chart as shown in Figure 8. Any optimization algorithm is built on the objective function and constraints.

2.3.1. Objective function

The target attribute or objective is to minimize THD. The THD value from the Simulink diagram is measured using the THD measurement block. The average value of the THD is taken here as the objective function. It can be represented as the following expression as given in (20). In (21) and (22) is the constraint that decides the gain values range in the optimization algorithm.

$$f\left(k_p, k_i\right) = \text{minimize}\ \left(\frac{\sum_{i=1}^{n} THD}{\text{total number of samples}}\right) \tag{20}$$

$$0 < k_p < 1200 \tag{21}$$

$$0 < ki < 1200 \tag{22}$$

The values of the final results from the simulation were not much when kp and ki varied more than 1,200. So the maximum value is selected here as 1,200. The gain values are populated and updated using the PSO algorithm and checked for the minimization of the objective function given in (20). The number of iterations is decided as per the convergence obtained from the PSO algorithm.

3. RESULTS AND DISCUSSION

In the MATLAB/Simulink environment, the suggested technique for creating PSO-PI controllers for DSTATCOM control is implemented. MATLAB's wind turbine model with a PMSM is used; it has a 300 V voltage rating and a 4,500-rpm rotational speed. The system's solar panel is a 1Soltech 1STH-245-WH, which has a 37.2 V open circuit voltage, a 30.2 V maximum power point voltage, and an 8.62 A short circuit current. The system includes both linear and non-linear loads, with the non-linear load being represented by an RLC configuration made up of a 20-ohm resistor, 0.1 H inductor, and a 500 uF capacitor. The suggested system's specifications are shown in Table 1.

Table 1. Specifications of proposed system

	Parameter	Value
Distribution system	Voltage	400 V
	frequency	50 Hz
	line R	0.001 ohm
	line L	0.05 mH
Linear load	Real power in W	5,000 W
	Reactive in VAR	3,000 MVar
Non-linear load	Resistance	20 ohms
	Inductance	0.1 H
	Capacitor	500 uF
PV specs	PV panel model name	1Soltech 1STH-245-WH
	open circuit voltage (Voc) V	37.2
	maximum power point voltage (V)	30.2
	short circuit current Isc (A)	8.62
	no, of parallel strings	2
	no. of series-connected modules per string	20
Wind generator specs	phase	3
	torque	6 Nm
	DC voltage	300 V
	speed in RPM	4,500

The study is initially conducted without the DSTATCOM and four cases are taken into consideration. A system without DSTATCOM is represented by case 1, a balanced loading situation with DSTATCOM is represented by case 2, a three-phase fault state with DSTATCOM is present in case 3, and an unbalanced loading condition with DSTATCOM is present in case 4. The transmission line's load bus system is coupled to the linear and nonlinear loads. To supply real power support for the DSTATCOM, PV, and wind power generation are implemented at the DC connection. By comparing the PI controller with the PSO-tuned PI controller, power quality and stability are assessed, as well as feasibility, by looking at power curves with faults and imbalanced loading. Figure 9 shows the convergence of the PSO algorithm. It can be seen that the final results of THD are shown as less at the 9th iteration. The convergence criteria taken here is when the results are nearly the same in consequent iterations. PSO algorithm thus used will progressively reduce the THD values for each iteration to obtain the global minima in the PI parameter estimation.
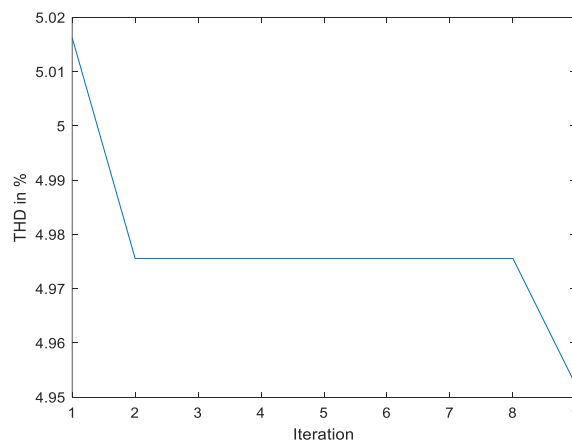

Figure 9. Convergence graph-PSO algorithm

3.1. Case 1: system with no DSTATCOM

The MATLAB Simulink-based simulation circuit is rigged up using the specifications mentioned in Table 1 without DSTATCOM. Without the DSTATCOM, Figure 10 displays the distribution system voltage and current characteristics. At 0.25 seconds, the DSTATCOM will be connected. Hence, the distribution system current of all three phases can be seen to be distorted for 0.25 seconds. The fast fourier transform (FFT) analysis of distribution system current as measured without DSTATCOM is shown in Figure 11. The figure makes it evident that the distribution system current's THD is 21.88%, which is extremely high.
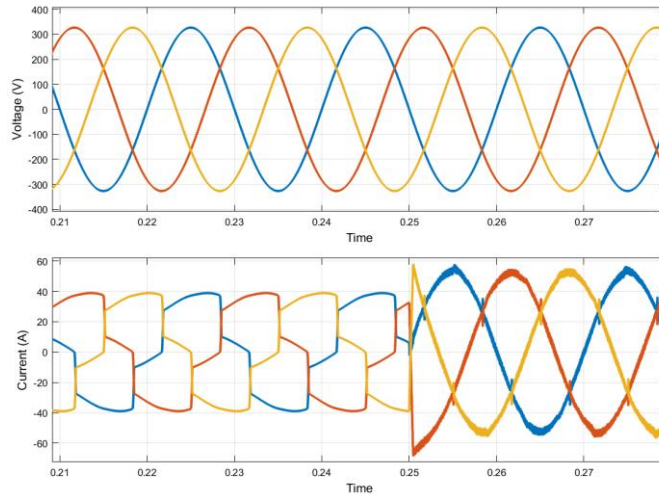
Figure 10. Voltage and current at distribution system-case 1 (STATCOM connected at 0.25 secs)
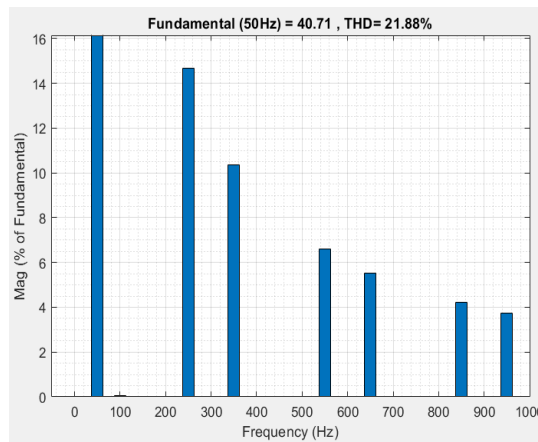
Figure 11. THD response-case 1

3.2. Case 2: balanced loading condition with D-STATCOM

Case 2 deals with the linear and non-linear loads that are connected to the transmission line's load bus system. For real power support for DSTATCOM, PV, and wind power generation are integrated at the DC link. Figure 12 displays the power factor in case 2 following the connection of DSTATCOM. It displays a unity power factor; however, PSO-PI performs better than PI.

Power regulation on the distribution system side is executed by applying the dq control with the conventional and PSO-PI controller. Figure 13 displays the actual distribution system side power in watts for case 2. In comparison to PI, the PSO-PI adds more power to the distribution system. It demonstrates that the PSO-PI injects 17.5 kW while the distribution system receives 16 kW. The distribution system's power injection is shown by the negative sign. The distribution system's reactive power in case 2 is then shown in Figure 14. Negative and nearly 0 in value, reactive power. It is positive in the PI controller, indicating that the compensation is not perfect. Figure 15 displays the actual power that the DSTATCOM in case 2 supplied.

It demonstrates how better DSTATCOM injection is in PSO-PI. Figure 16 displays the reactive power provided by DSTATCOM in case 2. Reactive power is again superior in comparison. Figures 17 and 18 show the FFT analysis for a proposed system with a conventional controller and PSO-PI controller respectively. The THD obtained is 2% less THD produced when the PSO-PI controller is used.
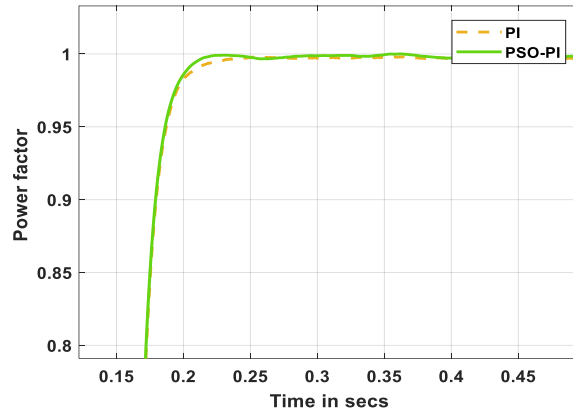
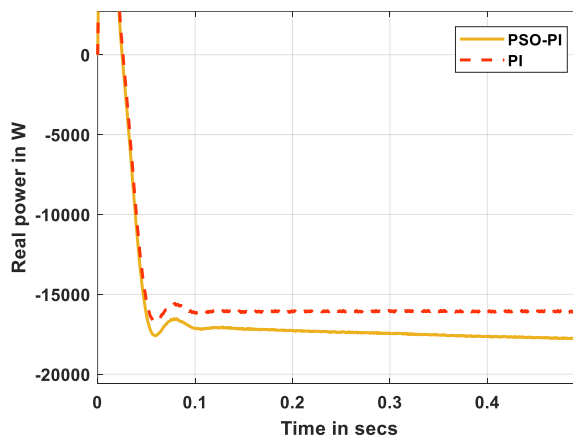Figure 12. Power factor with STATCOM connected-case 2
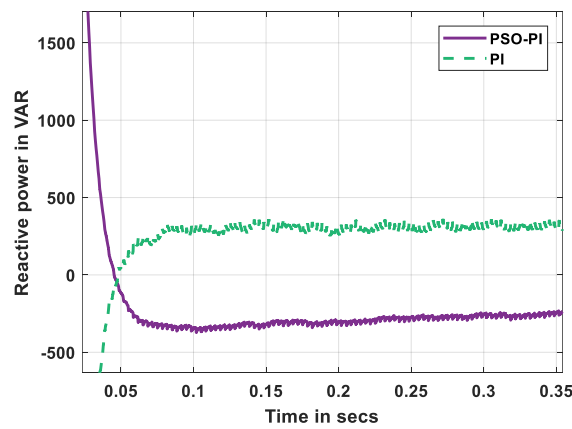
Figure 13. Real power-distribution system side-case 2

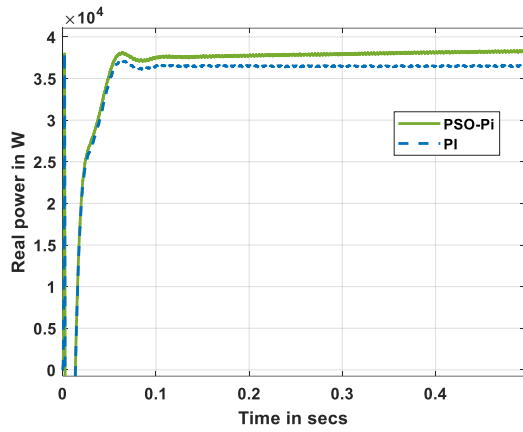Figure 14. Reactive power-distribution system side-case 2

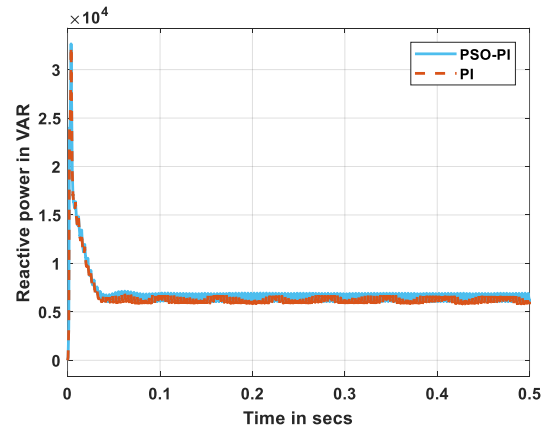Figure 15. Real power from STATCOM-case 2
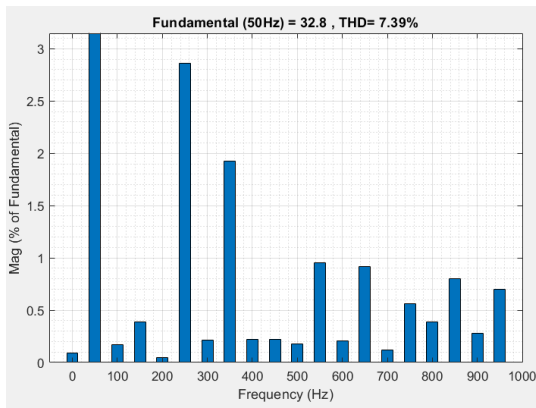

Figure 16. Reactive power from STATCOM-case 2

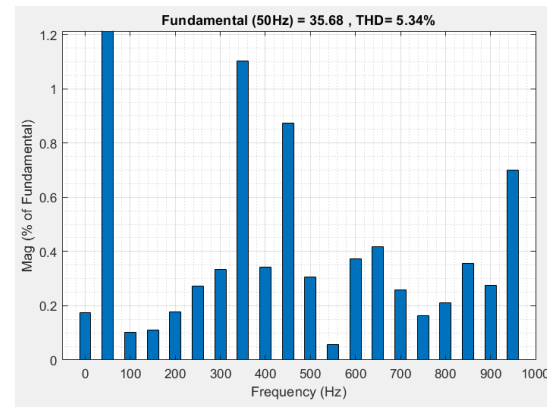Figure 17. Current THD with PI controller-case 2

Figure 18. Current THD with PSO-PI case 2

3.3. Case 3: three-phase fault condition with the presence of D-STATCOM

The real power on the distribution system in case 3 is depicted in Figure 19. The PSO-PI is also more effective at injecting power here. The actual power at DSTATCOM in case 3 is depicted in Figure 20. The reactive power at DSTATCOM in case 3 is also shown in Figure 21. When compared to PI in case 3, the PSO-PI injection of real and reactive power is superior. The power factor in example 3 is depicted in Figure 22.
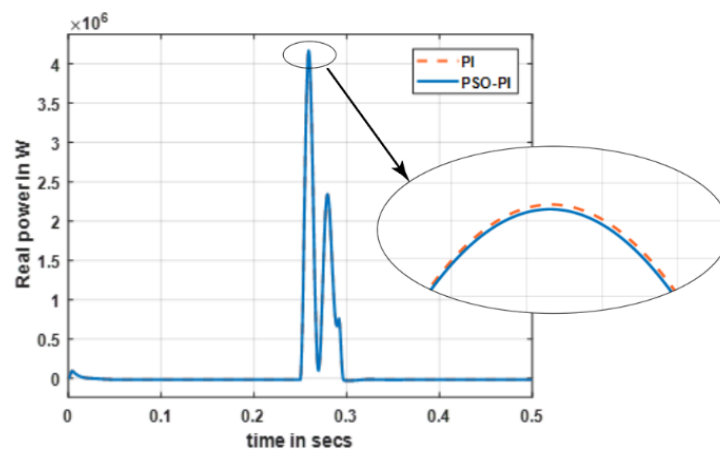

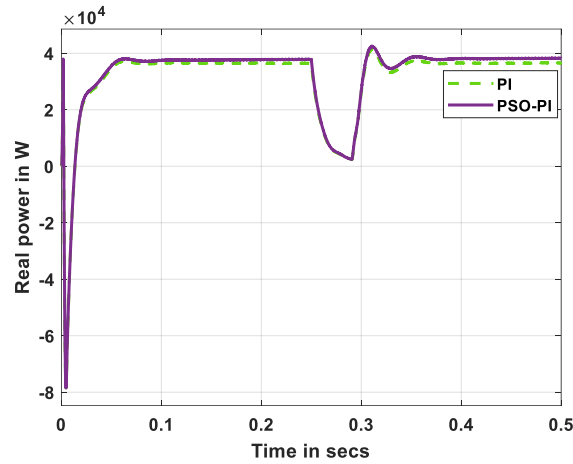Figure 19. Real power at the distribution system in case 3
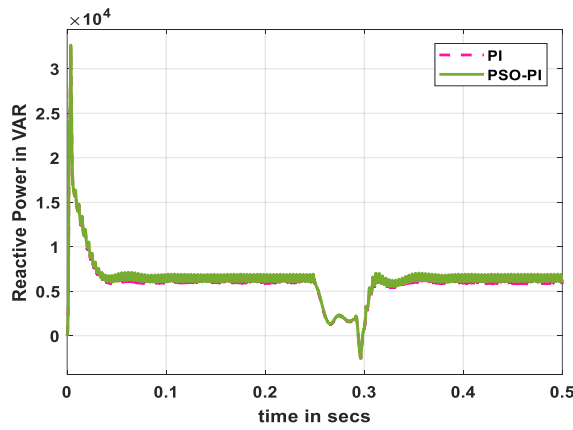

Figure 20. Real power at DSTATCOM in case 3
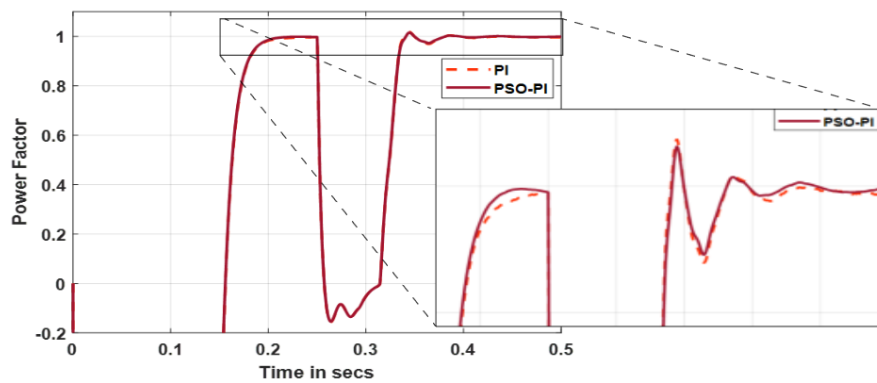

Figure 21. Reactive power at DSTATCOM in case 3

Figure 22. Power factor in case 3

3.4. Case 4: with DSTATCOM unbalanced loading condition

The distribution system voltage and current in case 4 are displayed in Figure 23. For the sake of simplicity and to prevent repeating figures, other results from case 4 are not included here. The results of the other power graphs are identical to those of cases 2 and 3. The performance of the proposed PSO PI was validated by comparing the results with an existing optimization approach. The specifications of wind turbine is tabulated in Table 2. The updated kp and ki values for Ziegler Nichols and PSO approaches are displayed

in Table 3. Active power, reactive power, THD, and power factor obtained for the proposed cases 1-4 with PSO and PSO-PI controller are given in Table 4. From the table, it can be inferred that PSO-PI gives better results when compared to the conventional tuning method.
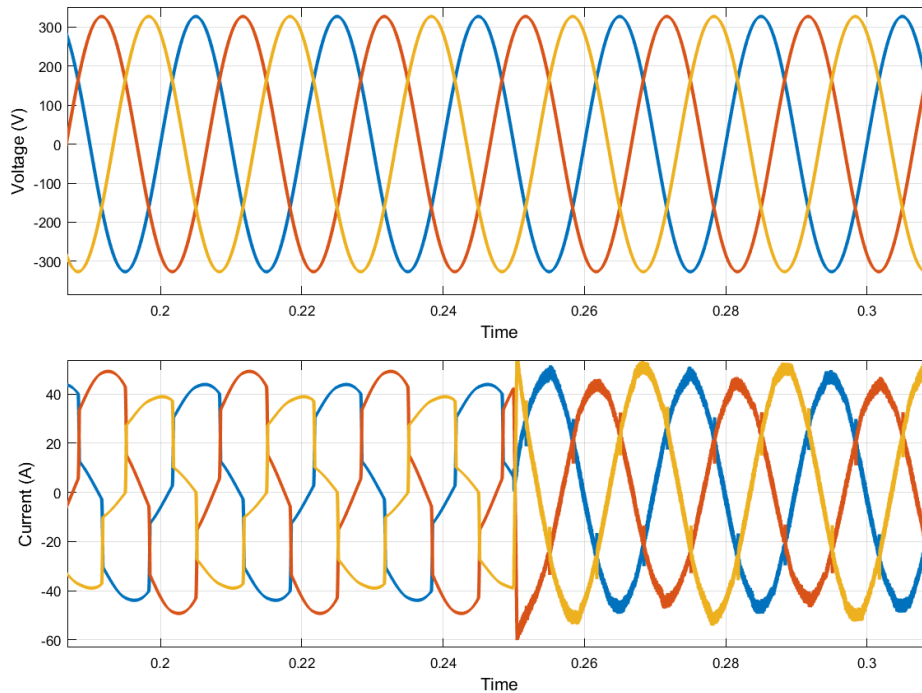

Figure 23. Voltage and current response in case 4

Table 2. Wind turbine parameters

PI controller	Speed (rpm)	Power (kW)
Case1	10	8.6
Case 2	15	12.4
Case 3	20	15.3

Table 3. Identified kp and ki parameters

PI controller		Zeigler Nichols method	PSO method
Case 1	Kp	800	1083.3
	Ki	120	1133.7
	Kp	800	1083.3
Case 2	Ki	120	1133.7

Table 4. Comparison of performance of the proposed system for four cases

Case	Active power (KW)		Reactive power (KVAR)		THD in (%)		Power factor	
	PI	PSO-PI	PI	PSO-PI	PI	PSO-PI	PI	PSO-PI
Case 1	50	50	50	50	21.88	5.69	0.7	0.99
Case 2	-16	-17	0.300	-0.300	7.39	5.34	0.99	0.99
Case 3	-16	-17	0.300	-0.300	7.39	5.34	0.99	0.99
Case 4	-16	-17	0.300	-0.300	7.39	5.34	0.99	0.99

Thus, the implementation of parameter estimation using PSO on the PI controller has improved both the THD and the power factor of the distribution system-connected PV system with DSTATCOM. Further analysis of the optimization can be checked with different ranges of gain values and different maximum numbers of iteration values. Additionally, newer optimization algorithms can be implemented for the optimization algorithm.

4. CONCLUSION

In order to explore the performance of a D-STATCOM system under various operating situations, this work integrated the particle swarm method coding with MATLAB simulations. Case 1 (no D-STATCOM), case 2 (D-STATCOM with balanced loading), case 3 (D-STATCOM with three-phase defective conditions), and case 4 (D-STATCOM with unbalanced loading) were the four cases considered in the analysis. Results from the use of the PSO-PI control indicated notable improvements for each condition's THD, power factor, real power injection, and reactive power injection. A 1.5 kW increase in power injection into the distribution system was also made possible by the adoption of the new control system. Additionally, the successful 2% reduction in harmonics was a noteworthy accomplishment. And in the future different optimization algorithms can be incorporated to obtain competitive results.

REFERENCES

[1] T. Eswaran and V. S. Kumar, "Particle swarm optimization (PSO)-based tuning technique for PI controller for management of a distributed static synchronous compensator (DSTATCOM) for improved dynamic response and power quality," *Journal of Applied Research and Technology*, vol. 15, no. 2, pp. 173–189, Apr. 2017, doi: 10.1016/j.jart.2017.01.011.

[2] C. H. Liu and Y. Y. Hsu, "Design of a self-tuning pi controller for a STATCOM using particle swarm optimization," *IEEE Transactions on Industrial Electronics*, vol. 57, no. 2, pp. 702–715, Feb. 2010, doi: 10.1109/TIE.2009.2028350.

[3] T. Karthik, M. Prathyusha, R. Thirumalaivasan, and M. Janaki, "Power quality improvement using DSTATCOM," in *2019 Innovations in Power and Advanced Computing Technologies, i-PACT 2019*, Mar. 2019, pp. 1–7, doi: 10.1109/i-PACT44901.2019.8960234.

[4] W. Rohouma, R. S. Balog, A. A. Peerzada, and M. M. Begovic, "D-STATCOM for harmonic mitigation in low voltage distribution network with high penetration of nonlinear loads," *Renewable Energy*, vol. 145, pp. 1449–1464, Jan. 2020, doi: 10.1016/j.renene.2019.05.134.

[5] M. Rastogi, A. Ahmad, and A. H. Bhat, "Performance investigation of two-level reduced-switch D-STATCOM in grid-tied solar-PV array with stepped P&O MPPT algorithm and modified SRF strategy," *Journal of King Saud University-Engineering Sciences*, vol. 35, no. 6, pp. 393–405, Sep. 2023, doi: 10.1016/j.jksues.2021.06.008.

[6] H. Bakir and A. A. Kulaksiz, "Modelling and voltage control of the solar-wind hybrid micro-grid with optimized STATCOM using GA and BFA," *Engineering Science and Technology, an International Journal*, vol. 23, no. 3, pp. 576–584, Jun. 2020, doi: 10.1016/j.jestch.2019.07.009.

[7] G. Isha and P. Jagatheeswari, "Optimal allocation of DSTATCOM and PV array in distribution system employing fuzzy-lightning search algorithm," *Automatika*, vol. 62, no. 3, pp. 339–352, Oct. 2021, doi: 10.1080/00051144.2021.1963080.

[8] I. Alsaidan, P. Chaudhary, M. Alaraj, and M. Rizwan, "An intelligent approach to active and reactive power control in a grid-connected solar photovoltaic system," *Sustainability (Switzerland)*, vol. 13, no. 8, p. 4219, Apr. 2021, doi: 10.3390/su13084219.

[9] A. Ramadan, M. Ebeed, and S. Kamel, "Performance assessment of a realistic egyptian distribution network including PV penetration with DSTATCOM," in *Proceedings of 2019 International Conference on Innovative Trends in Computer Engineering, ITCE 2019*, Feb. 2019, pp. 426–431, doi: 10.1109/ITCE.2019.8646473.

[10] Z. H. Saleh, Z. H. Ali, R. W. Daoud, and A. H. Ahmed, "A study of voltage regulation in microgrid using a DSTATCOM," *Bulletin of Electrical Engineering and Informatics*, vol. 9, no. 5, pp. 1766–1773, Oct. 2020, doi: 10.11591/eei.v9i5.2442.

[11] R. Chakrabarty and R. Adda, "Reduced switch single DC source cascaded H-bridge multilevel inverter based DSTATCOM," in *IECON Proceedings (Industrial Electronics Conference)*, Oct. 2019, vol. 2019-October, pp. 7074–7079, doi: 10.1109/IECON.2019.8927119.

[12] K. K. Prasad, H. Myneni, and G. S. Kumar, "Power quality improvement and PV power injection by DSTATCOM with variable DC link voltage control from RSC-MLC," *IEEE Transactions on Sustainable Energy*, vol. 10, no. 2, pp. 876–885, Apr. 2019, doi: 10.1109/TSTE.2018.2853192.

[13] M. Kamran, M. Mudassar, M. R. Fazal, M. U. Asghar, M. Bilal, and R. Asghar, "Implementation of improved perturb and observe MPPT technique with confined search space for standalone photovoltaic system," *Journal of King Saud University-Engineering Sciences*, vol. 32, no. 7, pp. 432–441, Nov. 2020, doi: 10.1016/j.jksues.2018.04.006.

[14] A. P. Kumar, G. S. Kumar, and D. Sreenivasarao, "Three-phase four switch DSTATCOM topologies with special transformers for neutral current compensation and power quality improvement," *IET Generation, Transmission and Distribution*, vol. 13, no. 3, pp. 368–379, Feb. 2019, doi: 10.1049/iet-gtd.2018.5841.

[15] M. Rastogi, A. Ahmad, and A. H. Bhat, "Power factor correction and power quality improvement of supply grid with self-supported transformer-less DSTATCOM for different control strategies," *International Journal of Industrial Electronics and Drives*, vol. 5, no. 2, p. 101, 2020, doi: 10.1504/ijied.2020.115576.

[16] P. S. Sikder and N. Pal, "Modeling of an intelligent battery controller for standalone solar-wind hybrid distributed generation system," *Journal of King Saud University-Engineering Sciences*, vol. 32, no. 6, pp. 368–377, Sep. 2020, doi: 10.1016/j.jksues.2019.02.002.

[17] K. Srikumar and C. Saibabu, "A system and novel methodology to track maximum power from photo voltaic system: a comparative and experimental analysis," *Journal of King Saud University - Engineering Sciences*, vol. 32, no. 7, pp. 442–458, Nov. 2020, doi: 10.1016/j.jksues.2018.02.006.

[18] K. Chenchireddy, V. Kumar, K. R. Sreejyothi, and P. Tejaswi, "A review on D-STATCOM control techniques for power quality improvement in distribution," in *Proceedings of the 5th International Conference on Electronics, Communication and Aerospace Technology, ICECA 2021*, Dec. 2021, pp. 201–208, doi: 10.1109/ICECA52323.2021.9676019.

[19] A. Bag, B. Subudhi, and P. K. Ray, "A combined reinforcement learning and sliding mode control scheme for grid integration of a PV System," *CSEE Journal of Power and Energy Systems*, 2019, doi: 10.17775/cseejpes.2017.01000.

[20] F. E. Alfaris and S. Bhattacharya, "Control and real-time validation for convertible static transmission controller enabled dual active power filters and PV integration," *IEEE Transactions on Industry Applications*, vol. 55, no. 4, pp. 4309–4320, Jul. 2019, doi: 10.1109/TIA.2019.2910782.

[21] P. Huang *et al.*, "A technical review of modeling techniques for urban solar mobility: solar to buildings, vehicles, and storage (S2BVS)," *Sustainability (Switzerland)*, vol. 12, no. 17, p. 7035, Aug. 2020, doi: 10.3390/su12177035.

[22] R. Panigrahi, S. K. Mishra, S. C. Srivastava, A. K. Srivastava, and N. N. Schulz, "Grid integration of small-scale photovoltaic systems in secondary distribution network-a review," *IEEE Transactions on Industry Applications*, vol. 56, no. 3, pp. 3178–3195, May 2020, doi: 10.1109/TIA.2020.2979789.
[23] C. M. N. Mukundan, Y. Singh, S. B. Q. Naqvi, B. Singh, and J. Pychadathil, "Multi-objective solar power conversion system with MGI control for grid integration at adverse operating conditions," *IEEE Transactions on Sustainable Energy*, vol. 11, no. 4, pp. 2901–2910, Oct. 2020, doi: 10.1109/TSTE.2020.2981356.
[24] P. Chaudhary and M. Rizwan, "Intelligent approach-based hybrid control algorithm for integration of solar photovoltaic system in smart grid environment," *IET Smart Grid*, vol. 2, no. 3, pp. 445–454, Sep. 2019, doi: 10.1049/iet-stg.2019.0055.
[25] A. Almutairi, A. G. Abo-Khalil, K. Sayed, and N. Albagami, "MPPT for a PV grid-connected system to improve efficiency under partial shading conditions," *Sustainability (Switzerland)*, vol. 12, no. 24, pp. 1–18, Dec. 2020, doi: 10.3390/su122410310.

BIOGRAPHIES OF AUTHORS

Parag Vijay Datar ⓘ 🇬 SC ◖ received a B.E. degree in Electrical and Electronics Engineering from Gogte Institute of Technology, Belagavi, affiliated with Visvesvaraya Technological University, Belagavi in 2003. M.E. Degree in Power Systems from Walchand College of Engineering, Sangli affiliated to Shivaji University, Kolhapur, Maharashtra. He is currently working towards a Ph.D. degree in the Department of Electrical and Electronics Engineering, GIT, Belagavi, Karnataka, India. His areas of interest include power systems, high-voltage engineering, and power quality. He can be contacted at email: pvdatar@git.edu.

Deepak Balkrishna Kulkarni ⓘ 🇬 SC ◖ obtained his B.E. and M.E. degrees from Walchand College of Engineering, Sangli, Maharashtra, India in 1986 and 1993 respectively and Ph.D. in the area of Power Quality from Visvesvaraya Technological University, Belagavi, Karnataka, India in 2012. His areas of interest include power quality, FACTS, HVDC transmission, and power systems. He can be contacted at email: dbkulkarni@git.edu.